Backbone Dynamics of the Major Coat Protein of Bacteriophage M13 in Detergent Micelles by ^{15}N Nuclear Magnetic Resonance Relaxation Measurements Using the Model-Free Approach and Reduced Spectral Density Mapping

Christina H. M. Papavoine, M. Lyndsay Remerowski,‡ Lennard M. Horstink, Ruud N. H. Konings, Cornelis W. Hilbers,* and Frank J. M. van de Ven§

Nijmegen SON Research Center, Laboratory of Biophysical Chemistry, University of Nijmegen, Toernooiveld 6525 ED Nijmegen, The Netherlands

Received October 22, 1996⊗

ABSTRACT: The backbone dynamics of the major coat protein (gVIIIp) of the filamentous bacteriophage M13, solubilized in detergent micelles, have been studied using ^{15}N nuclear magnetic resonance spectroscopy at three frequencies. Motional parameters and overall and internal correlation times were derived with the model-free approach. It was also checked whether these parameters had to be modified due to anisotropic motion of the protein/micelle complex. Reduced spectral density mapping was used to calculate the spectral densities at $J(0)$, $J(\omega_N)$, and $\langle J(\omega_H)\rangle$. The spectral densities were interpreted by mapping a linear or scaled linear combination of two Lorentzians onto a $J(0) - J(\omega)$ plot. The major coat protein of bacteriophage M13 consists of two α -helices, one of which is hydrophobic and located within the micelle, while the other is amphipathic and located on the surface of the micelle. Our results indicate that the motion of the hydrophobic helix is restricted such that it corresponds to the overall tumbling of the protein/micelle complex. The interpretation of the relaxation data of the amphipathic helix by means of the model-free approach and the reduced spectral density mapping indicate that in addition to the overall motion all residues in this helix are subject to motion on the fast nanosecond and picosecond time scales. The motions of the vectors in the low nanosecond range are characterized by similar values of the spectral densities and correlation times and represent the motion of the amphipathic helix on and away from the surface of the micelle. The relaxation data of the residues in the hinge region connecting the helices show that there is an abrupt change from highly restricted to less restricted motion. Both the C-terminal and N-terminal residues are very mobile.

The present paper focuses on the determination of the backbone dynamics of the gene VIII protein (gVIIIp)[1] encoded by the well-known filamentous bacteriophage M13. GVIIIp is a small protein (50 residues) that functions as the major coat protein in the phage particle and also as an intrinsic membrane protein during the life cycle of the phage. In the viral coat, 2700 copies of gVIIIp are arranged into a helical assembly with a 5-fold rotational axis and an almost 2-fold screw axis (Marvin et al., 1994). Although the phage particle is soluble in aqueous solution, the individual coat proteins are not.

The gene VIII protein has been investigated extensively. Due to its small size and its relatively facile isolation in large quantities, it has become a popular model system for studying membrane assembly (Wickner, 1988). Structural studies of the protein in the membrane-bound form or in membrane-mimicking environments have been undertaken by several groups (Van de Ven et al., 1993, Henry & Sykes, 1992; Opella et al., 1994). It has been found that in the micellar systems sodium dodecyl sulfate (SDS) and dodecylphosphocholine (DodPCho) the coat protein folds into a conformation consisting of two α-helices, connected by a hinge region located around residue 22. A hydrophobic helix, encompassing residues 25−45, spans the micelle, while an amphipathic helix (consisting of residues 6−20) is near the surface of the micelle (van de Ven et al., 1993; Papavoine et al., 1994, 1995). Similar results were obtained by solid-state NMR studies of the related bacteriophage fd coat protein bound to oriented bilayers (McDonnell et al., l993).

The dynamic properties of gVIIIp dissolved in detergent micelles, as well as in phospholipid bilayers, have been studied extensively by high-resolution NMR and solid-state NMR (Cross & Opella, 1980; Colnago et al. 1985; Leo et al., 1987; Bogusky et al., 1988; Henry et al., 1986, 1987a). The results of these, mostly one-dimensional, experiments showed that the terminal residues are mobile and the other residues are rigid on the NMR time scale. From spectra of selectively labeled samples recorded at 45 °C, Henry and Sykes (1992) showed smaller ^1H line widths for some N-terminal resonances, which were earlier found to be rigid (Henry et al., 1986). Finally, two-dimensional $^1H-^{15}N$ heteronuclear correlation spectra of the coat protein in SDS micelles recorded at 37−39 °C (Van de Ven et al., 1993), revealed for residues 24−45 ^{15}N line widths ranging from

* Address correspondence to this author. E-mail: ceesh@sci.kun.nl. Tel: 31-24-3652160/3652678. Fax: 31-24-3652112.

‡ Present address: Departement d'Ingenierie et d'Etudes des Proteines, Direction des Sciences Vivant, CE-Saclay, 91191 Gif-sur-Yvette Cedex, France.

§ Deceased on March 6, 1996.

⊗ Abstract published in *Advance ACS Abstracts,* March 15, 1997.

[1] Abbreviations: gVIIIp, gene VIII protein (major coat protein); SDS, sodium dodecyl sulfate; HSQC, heteronuclear single quantum shift correlation; DodPCho, dodecylphosphocholine; CPMG, Carr−Purcell−Meiboom−Gill; NMR, nuclear magnetic resonance; NOE, nuclear Overhauser enhancement; ppm, parts per million.

S0006-2960(96)02650-5 CCC: $14.00

15 to 20 Hz, whereas residues 6−20 had ^{15}N line widths of 5−10 Hz.

Additional dynamical information comes from the kinetics of hydrogen exchange at amide sites. Sykes and co-workers (Henry et al., 1987b; O'Neil & Sykes, 1988; Henry & Sykes, 1990) showed, by measuring the exchange rates of several amide protons throughout the protein, that the residues in the hydrophobic helix undergo very slow exchange, while the amide protons of the residues in the amphipathic helix exchange more rapidly.

In the present study, we present a full analysis of the backbone dynamics of almost all individual residues of gVIIIp in SDS and DodPCho micelles. This was achieved by ^{15}N spin-relaxation measurements using proton-detected two-dimensional (2D) $^{15}N-^{1}H$ NMR spectroscopy methods at three different spectrometer frequencies. The results, which were interpreted using the model-free approach, including the possibility of anisotropic motion, and using reduced spectral density mapping, show that the residues at both termini of gVIIIp are very flexible. Furthermore, the data show that the amphipathic helix exhibits motions on the fast nanosecond and picosecond time scales, superimposed on the overall motion of the complex. The motion of the residues in the hydrophobic helix is very much constrained; the motion of this helix is characterized by the overall motion of the protein/micelle complex.

MATERIALS AND METHODS

Sample Preparation. The filamentous M13 phages were propagated on Escherichia coli K38 grown in minimal medium as described previously (Konings, 1980). $^{15}NH_4Cl$ was used as the sole nitrogen source to obtain uniformly ^{15}N-labeled M13 phages. The isolation and purification of the phages were performed as described earlier (Konings, 1980; Spruyt et al., 1989). Separation of gVIIIp from the phage particles was carried out by phenol extraction (Knippers & Hoffman-Berling, 1966; Konings et al., 1970). The concentration of gVIIIp in the samples was typically 1.5−2.0 mM/500 mM [$^{2}H_{25}$]SDS (MSD Isotopes) or 1.5−2.0 mM/400 mM [$^{2}H_{38}$]DodPCho (Isotec Inc). The pH of the samples was 4.90 (pH meter reading).

NMR Spectroscopy. All NMR experiments were performed at 37 °C, using Varian Unity+ 500 and 750 spectrometers and a Bruker AMX600 spectrometer. The measurements at 500 MHz were repeated twice, several weeks apart. The pulse sequences used to measure ^{15}N R_1 and R_2 relaxation rates and the heteronuclear NOEs were based on those described previously by Dayie and Wagner (1994), which include pulsed-field gradients to select coherence-transfer pathways (Kay et al., 1992a) and the sensitivity-enhancement procedure developed by Cavanagh et al. (1991) and Palmer et al. (1991a,b). The water magnetization was returned to its equilibrium position (along the *z*-axis) prior to acquisition (Stonehouse et al., 1994). In the R_2 experiment a 90° ^{15}N pulse followed by the application of a gradient pulse is given at the beginning of the experiment, in order to ensure that the magnetization originates on ^{1}H and not on ^{15}N (Farrow et al., 1994). During the relaxation period in the R_2 experiment a CPMG-type sequence was used (Kay et al., 1992b; Palmer et al., 1992), in which the 139-μs 180° pulses were spaced 0.9 ms apart. Also, a series of $R_{1\rho}$ experiments was performed at 500 MHz. In the $R_{1\rho}$ experiments a 2.5-kHz spin-lock field was used during the relaxation period (Peng et al., 1991). Other parameters were the same as in the R_2 experiment. For the R_1 experiments, the phase of the 90° pulse before the relaxation period is alternated between y and $-y$ to ensure that the magnetization relaxes as $\exp(-T/T_1)$ (Kay et al., 1989).

All HSQC spectra, from which R_1 and R_2 were extracted, were collected with 512 t_1 increments and 2K real points in the t_2 dimension. The NOE spectra were recorded with 350 (500 MHz) and 512 (600 and 750 MHz) t_1 increments and 2K real points in the t_2 dimension. The sweep width was 12.0 ppm in the proton dimension and 22 ppm in the nitrogen dimension. A delay of 1.2 s was used between the acquisition steps in the R_1 and R_2 experiments, while a delay of 4.5 s (750 MHz) and 5.0 s (500 and 600 MHz) was used for the NOE experiments. Ten relaxation periods of 15, 45, 105, 195, 410, 605, 780, 995, 1295, and 2005 ms were used in the R_1 experiments. In the R_2 experiments relaxation periods of 8, 25, 41, 58, 72, 91, 124, 157, 240, and 322 ms were used. In the determination of $R_{1\rho}$, nine delays were used, ranging from 8 to 232 ms.

All data were processed using the MNMR program (PRONTO Software Development and Distribution, Copenhagen, Denmark) running on a Silicon Graphics Indigo workstation. The time domain data were zero-filled to 2048 and 4096 complex points in the t_1 and t_2 dimensions, respectively, and apodized using a cosine-bell function in the t_1 and a Lorentzian-to-Gaussian filtering function in the t_2 dimension. The spectra were analyzed using the program XEASY (Bartels et al., 1995).

Determination of the Relaxation Parameters. All relaxation parameters (R_1, R_2, $R_{1\rho}$, and NOE) were determined from the peak heights. Uncertainties in the measured peak heights due to noise were extracted from the root-mean-square (rms) baseline noise of the spectra. The individual R_1 and R_2 rate constants were obtained by fitting two- and three-parameter single-exponential functions to the experimental data using the methods of nonlinear least squares available in MATLAB (MathWorks, Inc.) (Nelders−Meade simplex algorithm) and Modelfree 3.1 (Mandel et al., 1995) (Levenburg−Marquardt algorithm) software. The results obtained via both programs were identical. The uncertainties in the rate constants were determined via Monte Carlo simulations using Modelfree 3.1 (Palmer et al., 1991b). The NOEs were determined by dividing the peak heights in the heteronuclear NOE enhancement spectra by those in the reference spectra. The uncertainties for the NOEs were calculated by using the relative errors of the peaks in these spectra.

Data Analysis. When the relaxation of the ^{15}N nucleus is predominantly caused by the dipolar interaction with its attached amide proton and by the anisotropy of its chemical shift, the relaxation data can be interpreted in terms of the motion of the $^{15}N-^{1}H$ vector. This motion is a superposition of both the overall motion of the protein and the motion of the vector itself. Relaxation processes restoring the equilibrium magnetization will be particularly effective if these motions take place at the resonance frequencies of the involved nuclei. The relationship between the relaxation parameters and the spectral density function $J(\omega)$ (which monitors the motional behavior of the $^{15}N-^{1}H$ vector) are given by (Abragam, 1961)

$$R_1 = d^2[3J(\omega_N) + 6J(\omega_H + \omega_N) + J(\omega_H - \omega_N)] + c^2J(\omega_N) \quad (1)$$

$$R_2 = (^1/_2)d^2[4J(0) + 3J(\omega_N) + 6J(\omega_H + \omega_N) + 6J(\omega_H) + J(\omega_H - \omega_N)] + (^1/_6)c^2[4J(0) + 3J(\omega_N)] + R_{ex} \quad (2)$$

$$\mathrm{NOE} = 1 + (\gamma_H/\gamma_N)d^2[J(\omega_H - \omega_N) - 6J(\omega_H + \omega_N)](1/R_1) \quad (3)$$

in which

$$d^2 = (^1/_4)\gamma_H{}^2\gamma_N{}^2h^2/(4\pi^2)\langle 1/r_{NH}{}^3\rangle^2 \quad (4)$$

$$c^2 = (^1/_3)\gamma_N{}^2B_0{}^2(\sigma_{||} - \sigma_\perp)^2 \quad (5)$$

where h is Planck's constant, γ_H and γ_N are the gyromagnetic ratios of the ^{1}H and ^{15}N nuclei, respectively, and ω_H and ω_N are the ^{1}H and ^{15}N Larmor frequencies, respectively; r_{NH} is the internuclear ^{15}N−^{1}H distance (1.02 Å), B_0 is the magnetic field strength, and $\sigma_{||} - \sigma_\perp$ is the difference between the parallel and perpendicular components of the axially symmetric ^{15}N chemical shift tensor, estimated to be −160 ppm (Hiyama et al., 1988). The exchange term, R_{ex}, has been included in eq 2 to account for chemical exchange processes.

Given that the three experimentally determined parameters, R_1, R_2, and NOE, depend on the spectral density function at five different frequencies, it is not possible to calculate the spectral density values at these frequencies without an assumption about the form of the spectral density function. This problem has been approached in two ways, first by the application of so-called reduced spectral density mapping, in which the relaxation rates are directly translated in the spectral density at three different frequencies, and second by use of a physical model to describe the spectral density function.

Reduced spectral density mapping, introduced by Farrow et al. (1995), Ishima and Nagayama (1995a,b), and Lefèvre et al. (1996), makes use of the finding that at high frequencies the spectral density function is quite flat, i.e., in the region of 500−700 MHz the $J(\omega)$ varies very slowly. At these conditions the three spectral densities $J(\omega_H + \omega_N)$, $J(\omega_H)$, and $J(\omega_H - \omega_N)$ may be averaged to one average spectral density $\langle J(\omega_H)\rangle$. Then the three relaxation rates in eqs 1−3 are sufficient to determine the spectral density values at $J(0)$, $J(\omega_N)$, and $\langle J(\omega_H)\rangle$ according to

$$\begin{bmatrix} J(0) \\ J(\omega_N) \\ \langle J(\omega_H)\rangle \end{bmatrix} = \begin{bmatrix} -3/4(3d^2 + c^2) & 3/2(3d^2 + c^2) & 9/10(3d^2 + c^2) \\ 1/(3d^2 + c^2) & 0 & -7/5(3d^2 + c^2) \\ 0 & 0 & 1/5d^2 \end{bmatrix} \begin{bmatrix} R_1 \\ R_2 \\ R(H_z{}^N \rightarrow N_z) \end{bmatrix} \quad (6)$$

where c^2 and d^2 are the constants defined in eqs 4 and 5. The magnetization transfer $R(H_z{}^N \rightarrow N_z) = d^2[J(\omega_H - \omega_N) - 6J(\omega_H + \omega_N)]$ is correlated with the NOE via eq 3. The frequency in the average spectral density, $\langle J(\omega_H)\rangle$, may be taken equal to $0.87\omega_H$ (Farrow et al., 1995).

An earlier, alternative approach to interpret the relaxation parameters is the widely used model-free approach of Lipari and Szabo (1982a,b). This interpretation can be "refined" by assuming that the overall motion is described by axially symmetric anisotropic tumbling of the protein (Woesner, 1962a,b; Schurr et al., 1994; Tjandra et al., 1995). Both models include fast internal motion of the ^{15}N−^{1}H bond, i.e., the overall and internal motions are treated as independent processes.

In the model-free approach, the spectral density function is described by

$$J(\omega) = (^2/_5)\left[\frac{S^2\tau_c}{1 + (\omega\tau_c)^2} + \frac{(1 - S^2)\tau'_e}{1 + (\omega\tau'_e)^2}\right] \quad (7)$$

where $\tau'_e = \tau_e\tau_c/(\tau_e + \tau_c)$, τ_c is the overall correlation time of the molecule, and τ_e is the effective correlation time for the internal motion. S^2 is the generalized order parameter which is a measure of the degree of spatial restriction of the ^{15}N−^{1}H bond. It has values between 0 and 1, indicating completely unrestricted and completely restricted motion, respectively.

The spectral density function in the model-free approach has been extended to account for the presence of separate internal motions on slow and fast time scales (Clore et al., 1990a,b). In this approach, the faster internal correlation time is assumed to be so short (<10 ps), that the extended model-free spectral density function can be described by

$$J(\omega) = (^2/_5)\left[\frac{S_f{}^2S_s{}^2\tau_c}{1 + (\omega\tau_c)^2} + \frac{S_f{}^2(1 - S_s{}^2)\tau'_e}{1 + (\omega\tau'_e)^2}\right] \quad (8)$$

$S_f{}^2$ and $S_s{}^2$ are the generalized order parameters of the internal motion on the fast ($S_f{}^2$) and slow ($S_s{}^2$) time scales, respectively and $S_f{}^2S_s{}^2 = S^2$. Here, τ'_e is defined as in eq 7 but now τ_e is the effective correlation time for the slow internal motion, which still needs to be appreciably faster than the overall motion.

For anisotropic axially symmetric tumbling of the protein, the spectral density function is related to two rotational diffusion constants, $D_{||}$ and $D_\perp$, for diffusion parallel and perpendicular to the cylindrical symmetry axis of the molecule (Woesner 1962a; Schurr et al., 1994):

$$J(\omega) = (^2/_5)\left\{S^2\left[\frac{C_1\tau_1}{1 + (\omega\tau_1)^2} + \frac{C_2\tau_2}{1 + (\omega\tau_2)^2} + \frac{C_3\tau_3}{1 + (\omega\tau_3)^2}\right] + (1 - S^2)\left[\frac{C_1\tau'_1}{1 + (\omega\tau'_1)^2} + \frac{C_2\tau'_2}{1 + (\omega\tau'_2)^2} + \frac{C_3\tau'_3}{1 + (\omega\tau'_3)^2}\right]\right\} \quad (9)$$

with

$$C_1 = {}^3/_4\sin^4\theta \qquad C_2 = 3\sin^2\theta\cos^2\theta \qquad C_3 = {}^1/_4(3\cos^2\theta - 1)^2$$

where θ is the angle between the ^{15}N−^{1}H internuclear vector and the unique axis of the molecule and $\tau'_i = \tau_e\tau_i/(\tau_e + \tau_i)$, with $\tau_i = \tau_1, \tau_2, \tau_3$. The correlation times τ_1, τ_2, and τ_3

Table 1: Models Used for Fitting[a]

approach	model	eq used	variables	constants
residues	1	7	S^2	$\tau_c = 11.8$ ns, $\tau_e = 0$
	2	7	S^2, τ_e	$\tau_c = 11.8$ ns
	3	8	S_s^2, τ_e, S_f^2	$\tau_c = 11.8$ ns
	4	7	S^2, R_{ex}	$\tau_c = 11.8$ ns, $\tau_e = 0$
	5	7	S^2, τ_e, R_{ex}	$\tau_c = 11.8$ ns
helices	I	7	τ_c	$\tau_e = 0$
	II	7	τ_c, S^2	$\tau_e = 0$
	III	7	τ_c, S^2, τ_e	
	IV	8	τ_c, S_s^2, τ_e, S_f^2	
	V	9	τ_{eff}, S^2, τ_e, r, θ	
	VI	9	τ_{eff}, S^2, r, θ	$\tau_e = 0$

[a] The R_1, R_2, and NOE data, measured at 500, 600, and 750 MHz, were used for all models. For models 1−5, the Modelfree 3.1 software was used. For models I−VI, the parameters used in the grid search using MATLAB were varied as follows: τ_c, $\tau_{eff} = 6.5-0.5-13$ ns, $S^2 = 0.4-0.05-1$, $\tau_e = 0-100-2000$ ps, $S_s^2 = 0.4-0.05-1$, $S_f^2 = 0.8-0.025-1$, $r = 1-0.5-5$ and $\theta = 0-10-90$, where the first number is the starting value, the second is the increment, and the last is the final value of the variable in the grid search.

depend on the rotational diffusion coefficients as follows:

$$\tau_1 = \frac{1}{4D_{\|} + 2D_{\perp}} \qquad \tau_2 = \frac{1}{D_{\|} + 5D_{\perp}} \qquad \tau_3 = \frac{1}{6D_{\perp}}$$

In the determination of the motional parameters, an anisotropy ratio, r, and an effective global correlation time, τ_{eff}, are used instead of $D_{\|}$ and $D_{\perp}$. These parameters are defined as $r = D_{\|}/D_{\perp}$ and $\tau_{eff} = 1/D_{eff}$, where $D_{eff} = {}^1/_3(D_{\|} + 2D_{\perp})$. In the case where $r = 1$, eqs 9 and 7 are identical.

The values of the motional parameters of the individual residues were derived following established approaches. Once the overall tumbling time τ_c has been determined, S^2, τ_e, S_s^2, S_f^2, and R_{ex} can be derived from eqs 1−3, 7, and 8. To determine the initial overall rotational correlation time the mean value of R_2/R_1 was used (Kay et al., 1989). In this procedure only residues with an NOE higher than 0.6 are included, since in this case the fast internal motions are unlikely to make significant contributions to the R_1 and R_2 relaxation rates. Subsequently, the other motional parameters for each individual residue were determined from the R_1, R_2, and NOE data, obtained at three spectrometer frequencies simultaneously in steps of increasing complexity. Thus, in the first step only S^2 was varied to obtain an optimal fit to the experimental data. In the second step, S^2 and τ_e were varied for this purpose, etc. These steps are represented by models 1−5 in Table 1. Optimal fits were obtained by minimizing the error function:

$$\chi^2 = \sum_{i=1}^{3}\left(\frac{R_{1,i}^{calc} - R_{1,i}^{meas}}{\sigma_{R_{1,i}}}\right)^2 + \left(\frac{R_{2,i}^{calc} - R_{2,i}^{meas}}{\sigma_{R_{2,i}}}\right)^2 + \left(\frac{NOE_i^{calc} - NOE_i^{meas}}{\sigma_{NOE_i}}\right)^2 \quad (10)$$

in which i denotes the proton resonance frequency of the spectrometer (1 = 500 MHz, 2 = 600 MHz, 3 = 750 MHz), the superscript meas refers to the measured data, and calc refers to the calculated values on the basis of eqs 7 or 8. The σ values are the uncertainties of the measured parameters. Minimization was achieved through a restrained nonlinear least-squares optimization using the Modelfree 3.1 software.

After having obtained the appropriate model for the individual residues within the simple and extended model-free approach (eqs 7 and 8), the overall correlation time was optimized simultaneously with the motional parameters obtained for all individual residues. The final calculation used 500 Monte Carlo simulations to determine uncertainties.

The relaxation data were also interpreted in terms of a model in which axially symmetric anisotropic tumbling of the protein/micelle complex was assumed. To simplify the calculations, the helices were assigned motional parameters. This is allowed because the relaxation data of the residues within each helix are similar. The helical motional parameters were calculated from the mean values of R_1, R_2, and NOE of the residues within each helix for each spectrometer frequency (*vide infra*). These mean values were used to obtain motional parameters for both isotropic and anisotropic tumbling. Again the different motional parameters were obtained in steps of increasing complexity. These steps are represented in Table 1 as well by models I− VI. The motional parameters were again determined by minimizing eq 10. Now, the calculated parameters were based on eqs 7, and 8 or eq 9. The minimization was performed using a grid search procedure in the program MATLAB. The first set of calculations (models I−IV) served to check the validity of the use of the average relaxation parameters by comparison with the results obtained with the Modelfree 3.1 software. The overall correlation time was not set to an initial value but was used as a variable in the grid search. The parameters were varied as follows: τ_c and τ_{eff} from 6.5 to 13 ns in steps of 0.5 ns, S^2 and S_s^2 from 0.4 to 1 in steps of 0.05, τ_e from 0 to 2000 ps in steps of 100 ps, S_f^2 from 0.8 to 1 in steps of 0.025, r from 1 to 5 in steps of 0.5 and θ from 0 to 90° in steps of 10°. The exchange term, R_{ex}, was not used in these grid search, for reasons explained in the Results and Discussion section.

The models (Table 1) were selected as follows: for each model, the number of statistical degrees of freedom (ν), defined as $M - p$, is determined. M is the total number of the relaxation parameters used (here $M = 9$ per residue or helix) and p is the number of motional parameters in the used model. To select the most appropriate model, the minimal value of the χ^2 in eq 10 was compared with 95% confidence interval, the $\alpha = 0.05$ critical value, of the χ^2 distribution. The latter was obtained from Monte Carlo simulations using the Modelfree 3.1 software (Palmer et al., 1991b; Mandel et al., 1995) or from statistics [Table A6 in Devore (1982)]. The critical values of both methods were similar. For all models we have fit the least number of parameters that are consistent with the data within experimental error.

A model was selected for a residue or helix if χ^2 was less than the critical value. A more complex model (more parameters) was selected if χ^2 was larger than the appropriate critical value and if this more complex model could be statistically justified. This justification can be done in terms of the statistical F-test (Devore, 1982). The F-test statistic is defined by

$$F = \frac{\nu_2(\chi_1^2 - \chi_2^2)}{(\nu_1 - \nu_2)\chi_2^2} \quad (11)$$

where χ_1^2 and χ_2^2 are the values for the models with ν_1 and

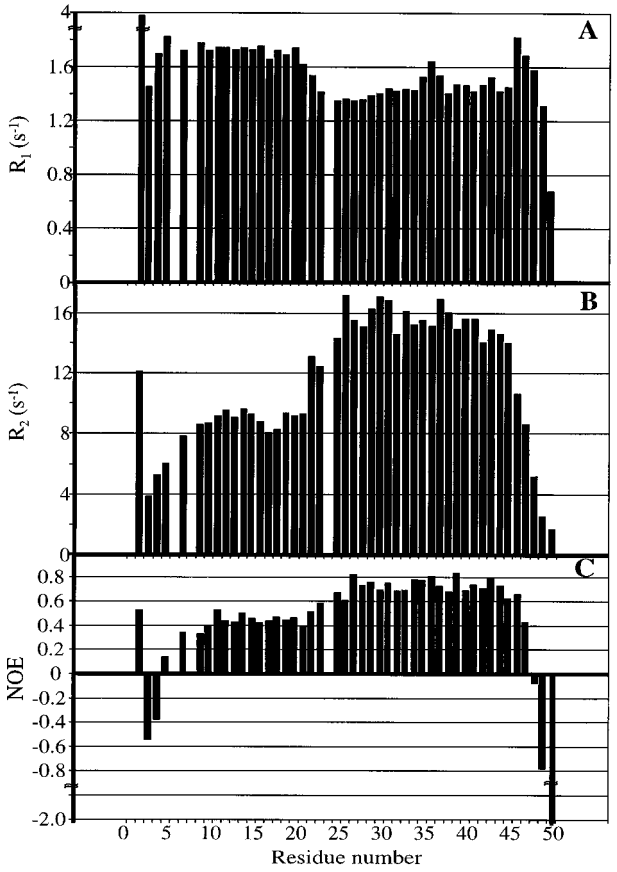

FIGURE 1: Experimental ^{15}N relaxation rates (A and B) and heteronuclear NOEs (C) versus residue number for gVIIIp in SDS micelles, obtained from the measurements at 500 MHz.

ν_2 degrees of freedom ($\nu_1 > \nu_2$). If the *F*-test statistic comparing two models is greater than the appropriate critical value, $F(\alpha, \nu_1 - \nu_2, \nu_2)$, the more complex model is used. α is the critical value of the *F* distribution and was set at 0.05; thus a more complex model is statistically justified if the value determined lies within the 95% confidence interval of the *F* distribution. This procedure was carried out for every added parameter. If the χ^2 of the most complex model still was higher than the appropriate critical value, the motional parameters were obtained from fitting the data with this model.

RESULTS AND DISCUSSION

R_1, R_2, and NOE Relaxation Data. In the present paper, use is made of the complete ^{15}N and NH resonance assignments for gVIIIp in SDS micelles reported earlier (Henry & Sykes 1992; Van de Ven et al., 1993). From the $^1H-^{15}N$ heteronuclear correlation experiments, the relaxation parameters of residues A1, P6, K8, and Y24 could not be determined. The first two of these amino acids do not give rise to a cross-peak in this type of spectra, and the cross-peaks of residues K8 and Y24 overlap too much to permit reliable measurements of the peak heights.

Figure 1 presents the R_1 (Figure 1A) and R_2 relaxation rates (Figure 1B) as well as the heteronuclear NOEs (Figure 1C) determined from the measurements performed at 500 MHz. The relaxation parameters obtained from the experiments at the other frequencies yielded the same global picture, although the absolute values were different because of the frequency difference. A complete list of the relaxation parameters for gVIIIp in SDS micelles is summarized in the supporting information. The mean values of the relaxation parameters obtained for gVIIIp in SDS micelles are presented in Table 2. The average uncertainty is 6.8% for R_1 and 6.7% for R_2. The average uncertainty in the NOEs is 13.0%; the uncertainty for $R_{1\rho}$ is 3.6%.

Table 2: Mean ^{15}N R_1 and R_2 ($R_{1\rho}$) Relaxation Data and NOEs and Their Standard Deviations at 500-, 600-, and 750-MHz Spectrometer Frequencies

frequency	R_1 (s^{-1})	dR_1 (s^{-1})	R_2 ($R_{1\rho}$) (s^{-1})	dR_2 (d$R_{1\rho}$) (s^{-1})	NOE	SD_{NOE}
500	1.58	0.06	11.46 (10.98)	0.79 (0.40)	0.58	0.06
600	1.31	0.09	11.60	1.02	0.62	0.10
750	1.11	0.10	13.90	0.62	0.67	0.07

In Figure 1, clear differences can be distinguished between the relaxation results in different regions of the protein. At the termini, residues 3−5 and 48−50 have small transverse relaxation rate constants and the heteronuclear NOE for these residues has a negative or small positive value. Furthermore, two regions can be distinguished, comprising residues 9−21 and 25−45, respectively, which exhibit distinct relaxation behavior. This difference is particularly manifest in the R_2 relaxation rate constants and the heteronuclear NOEs. In Figure 1B, it can be seen that the R_2 values of residues 25−45 are twice as large as those of residues 9−21. For the measurements performed at 500 MHz, the NOEs of the residues in the latter region are between 0.37 and 0.49, whereas the NOEs of residues 25−45 have an average value of about 0.74 (see Figure 1C). For the R_1 relaxation rate constants the difference between these two regions is smaller (R_1^{avg} (residues 9−21)= 1.7, R_1^{avg} (residues 25−45) = 1.4). The experiments performed at 600 and 750 MHz show similar differences between the relaxation parameters of the termini and the two regions described above. The relaxation data of gVIIIp in DodPCho micelles, measured at 500 MHz, are similar to those of gVIIIp in SDS micelles (data not shown). For residues 25−45 the R_2 relaxation rate is about twice as large as that of residues 6−20, whereas the NOEs in the latter region have smaller values than those of residues 25−45. However, the intensity of the peaks for these residues in the spectra of gVIIIp in DodPCho micelles was too low to perform a quantitative interpretation of the data.

As has been mentioned earlier, residues 6−20 form the amphipathic helix, while residues 25−45 correspond to the hydrophobic helix. Apparently, the dynamic behavior of these two helices is rather distinct. To obtain more detailed information on the origin of this difference and a better understanding of the dynamics of the total protein, motional parameters have been extracted from the relaxation parameters for gVIIIp in SDS micelles.

Determination of the Motional Parameters of Each Individual Residue: Model-Free Approach. The $^{15}N-^1H$ NOEs of residues 25−45 exceed the value of 0.6 and therefore, in a first approximation, the overall isotropic rotational correlation time was deduced from the average value R_2/R_1 of these residues (Kay et al., 1989). The heteronuclear NOEs of the other residues were below 0.6 and thus excluded from the τ_c determination. The average ratios obtained at 500, 600, and 750 MHz are $(R_2/R_1)_{500} = 10.81 \pm 0.20$, $(R_2/R_1)_{600} = 13.47 \pm 0.38$, and $(R_2/R_1)_{750} = 22.00 \pm 0.67$. These values correspond with τ_cs of 12.1 ± 0.1 ns (500 MHz), 11.4 ± 0.2 ns (600 MHz), and 11.9 ±

Table 3: Backbone Dynamical Parameters for the Individual Residues of gVIIIp[a]

residue no.	S^2	dS^2	τ_e (ps)	dτ_e (ps)	S_s^2	dS_s^2	S_f^2	dS_f^2	χ^2
Asp 4	0.22	0.02	938	17	0.24	0.01	0.90	0.01	10.41
Asp 5	0.27	0.04	1312	52	0.31	0.01	0.88	0.02	7.04
Ala 7	0.44	0.03	1278	57	0.51	0.01	0.86	0.01	41.86
Ala 9	0.47	0.03	1560	97	0.54	0.01	0.86	0.01	38.64
Ala 10	0.49	0.02	1572	87	0.57	0.01	0.86	0.01	22.24
Phe 11	0.51	0.04	1713	167	0.59	0.02	0.86	0.02	5.18
Asn 2	0.55	0.03	1690	154	0.62	0.02	0.89	0.02	4.45
Ser 13	0.51	0.03	1592	113	0.60	0.01	0.86	0.02	11.44
Leu 14	0.53	0.04	1716	201	0.60	0.02	0.88	0.02	10.55
Gln 15	0.53	0.03	1502	99	0.60	0.01	0.88	0.02	5.96
Ala 16	0.48	0.03	1564	114	0.56	0.02	0.85	0.02	11.76
Ser 17	0.45	0.03	1533	92	0.56	0.01	0.80	0.01	31.46
Ala 18	0.49	0.02	1573	78	0.58	0.01	0.85	0.01	46.86
Thr 19	0.55	0.04	1266	80	0.61	0.02	0.90	0.02	22.10
Glu 20	0.52	0.03	1467	98	0.58	0.02	0.90	0.02	23.19
Tyr 21	0.53	0.05	1523	166	0.63	0.02	0.84	0.02	15.76
Ile 22	0.83	0.03	969	175					6.70
Gly 23	0.89	0.03							17.22
Ala 25	0.90	0.02							20.70
Trp 26	0.97	0.03							11.47
Ala 27	0.97	0.04							9.69
Met 28	0.92	0.02							7.43
Val 29	0.97	0.03							7.85
Val 30	0.99	0.03							8.42
Val 31	1.00	0.03							7.92
Ile 32	0.96	0.03							4.16
Val 33	0.99	0.03							6.15
Gly 34	0.98	0.03							5.65
Ala 35	0.98	0.03							1.77
Thr 36	1.00	0.03							10.01
Ile 37	1.00	0.04							3.25
Gly 38	0.98	0.03							5.00
Ile 39	0.96	0.03							13.19
Lys 40	0.97	0.02							2.84
Leu 41	0.94	0.03							2.94
Phe 42	0.94	0.03							1.71
Lys 43	0.95	0.03							8.45
Lys 44	0.93	0.02							13.90
Phe 45	0.90	0.02	93	36					3.08
Thr 46	0.67	0.02	1465	117					21.29

[a] The parameters were determined from models 1−5.

0.2 ns (750 MHz). The average initial estimate of τ_c was set at 11.8 ± 0.4 ns. This correlation time is expected for a globular protein with a molecular mass of about 20−25 kDa, which is in good agreement with our earlier findings that one gVIIIp molecule (molecular mass = 5.2 kDa) is complexed with about 60 SDS molecules (Papavoine et al., 1994). Although the data of the residues of gVIIIp in DodPCho micelles only allow a qualitative interpretation, the average ratio $(R_2/R_1)_{500}$ of the residues of gVIIIp in DodPCho micelles is higher than that obtained for the protein/SDS system. This implies that a DodPCho micelle is larger in size than an SDS micelle, corresponding with a higher rotational correlation time.

Using this approximate correlation time, the motional parameters S^2, τ_e, S_s^2, and S_f^2 were derived along the lines indicated in the Materials and Methods section; they are listed in Table 3. Inspection of Table 3 shows that only one parameter, S^2, suffices to account for the observed relaxation behavior of residues 23−44. For three residues, i.e., 22, 45 and 46, two parameters, S^2 and τ_e, are needed, while the majority of the remaining residues required three parameters, S_s^2, τ_e, and S_f^2, to obtain a reasonable fit. The behavior of the terminal residues, 2−3 and 47−50, could not be described with any of the models 1−5 in Table 1 and were

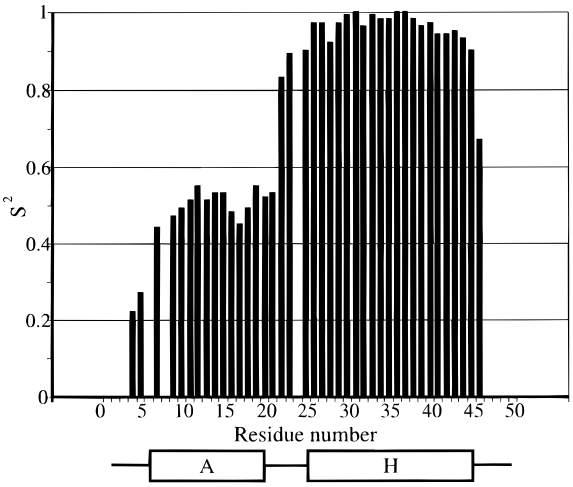

FIGURE 2: Plot of the order parameters S^2 as a function of residue number for gVIIIp in SDS micelles. The secondary structure of gVIIIp is indicated; the box with letter A denotes the amphipathic helix and the box with letter H the hydrophobic helix.

therefore excluded from the subsequent final calculations (*vide infra*). However, the relaxation parameters of these residues show that they are very mobile compared to the other residues in the molecule (smaller R_2s and small or negative NOEs except for residue 2, which will be discussed below). It is noted that the value of the 95% confidence interval of the χ^2 distribution, used in the fitting procedure, is 15.507, 14.067, and 12.592 for one, two, and three motional parameters, respectively (Devore, 1982, Table A6; it is noted that the total number of relaxation parameters available is 9). The use of an increasing number of motional parameters was justified according to the *F*-test statistic (see Materials and Methods). Using the number of motional parameters that were chosen for residues 4−46, the final value of τ_c calculated was 11.77 ± 0.08 ns.

Figure 2 displays the order parameters, S^2, of residues 4−46. A significant difference is observed for the residues within the two helices (A and H, see Figure 2); the average S^2 value of the amino acids in the hydrophobic helix is 0.96 (SD 0.03). This value corresponds with highly restricted internal motion in this part of the protein; earlier we have shown that this part of the protein traverses the micelle (Papavoine et al., 1994). Interestingly, this hydrophobic helix within the micelle exhibits dynamical properties similar to helices within the interior of globular proteins. The hinge region, which connects the two helices, is located around residue 22 (Van de Ven et al., 1993; Papavoine et al., 1994). For this residue S^2 is 0.83, and its internal motion is on the nanosecond time scale (τ_e = 969 ± 175 ps). Comparison of these dynamical parameters with those of residues 21 and 23 indicates that the motion of the residues closer to the hydrophobic helix becomes more restricted (higher S^2), whereas the residues closer to the amphipathic helix are more mobile (lower S^2, see Figure 2). In other words, the transition of the hydrophobic to the amphipathic helix, described in terms of dynamics, is characterized by a sudden change from very restricted to a much more unrestricted internal motion. The residues in the amphipathic helix, which is located on the surface of the micelle, have an average S^2 value of 0.51 (SD 0.03), showing much mobility on both the picosecond and the nanosecond time scales, with an average correlation time of the slow internal motion of 1560 ± 117 ps and a fast internal motion which is less than 10 ps. The high χ^2

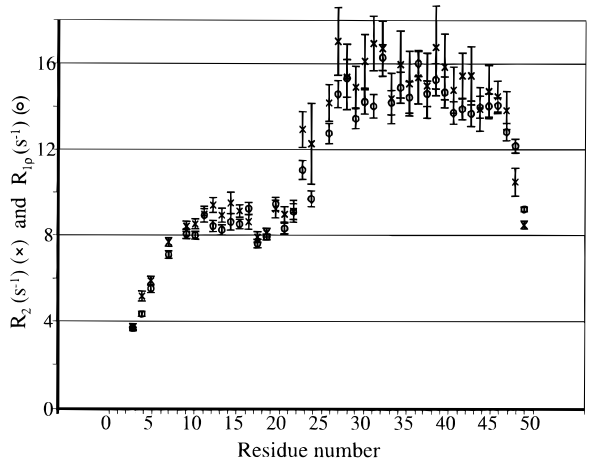

FIGURE 3: R_2 (×) and $R_{1\rho}$ (○) relaxation rates and uncertainties versus the residue number for gVIIIp in SDS micelles. The data were obtained from measurements performed at 500 MHz.

values of some residues (7, 9, 17, and 18) is an indication that the dynamics in this part of the protein might be more complex than represented by the models being applied here (see Table 3).

At both the N- and C-terminal parts of the protein, a "mobility gradient" is observed. At the N-terminus, the order parameters of residues 4 and 5 show that the motion of these amides is less restricted than the residues in the amphipathic helix. The motion of residues 2 and 3 is too complicated, so that it cannot be described with the models used, but the smaller R_2 and negative NOE of residue 3 are strong indications that this residue is more mobile than residues 4 and 5. The relaxation data of residue 2 for gVIIIp in SDS micelles (large R_1, R_2, and $R_{1\rho}$ and small positive NOE) is very different from that of the other terminal residues, which show small R_1 and R_2 values and negative NOEs. The origin of this is unclear. For gVIIIp in DodPCho micelles, the R_1 relaxation rate and heteronuclear NOE of residue 2 are similar to those of the other terminal residues. However, the R_2 relaxation rate of residue 2 in this system is still higher in comparison with the other terminal residues (data not shown). At the C-terminus, residues 45 and 46 show more mobility than the residues of the hydrophobic helix. However, in comparison with the N-terminus, the motion of these amides is more restricted. The relaxation parameters of residues 47−50 indicate, like those of residue 3, that they are very mobile.

Slow Conformational Exchange. For all residues, the addition of an exchange term, did not lead to a significantly better fit of the data. Normally, residues having a R_2/R_1 value that is one standard deviation greater than the average value are considered for addition of an exchange term (Clore et al., 1990a). For the determination of the average R_2/R_1 ratio, the values of residues 25−45 were used. For these residues only one parameter is sufficient to fit the data (*vide supra*). The R_2/R_1 of all other residues is almost a factor of 2 smaller than the average. An exchange term is thus not expected for these residues.

To further exclude the possibility that the R_2 of residues 25−45 might have an R_{ex} contribution and that the actual R_2/R_1 (and thus τ_c) is smaller than the value determined, we measured $R_{1\rho}$. Figure 3 displays both the R_2 and $R_{1\rho}$ values measured at 500 MHz. Comparison of the R_2 and $R_{1\rho}$ data, the latter obtained with a 2.5-kHz spin-lock field, show good agreement for residues 3−21. For residues 22−45, $R_{1\rho}$ is somewhat smaller than R_2 but for most residues the differences between the R_2 and $R_{1\rho}$ fall within their experimental error [for residues 25−45, the average $(R_2 - R_{1\rho}) = 1.01$ and the average dR_2 1.26]. Exceptions are the R_2s of residues 22−26 and 28−30. Excluding the R_2 of these residues from the mean determination lowers the τ_c with only 0.1 ns. Using only the $R_{1\rho}$ values for the determination of the correlation time lowers the τ_c with 0.5 ns. When the average correlation time was lowered to a value of 11.3 ns, the relaxation parameters of residues 23−44 could still be fitted by only varying S^2 and did not require an exchange term. For residues 22 and 25, an exchange term did not improve the fit significantly as well. From these observations, it has been concluded that residues 22−45 may have a small conformational exchange contribution, but the effect on the transverse relaxation rate is such that it does not influence the determined motional parameters. For this reason, the exchange term has not been included in the grid search for models I−VI, which are discussed below.

Table 4: Mean ^{15}N R_1 and R_2 Relaxation Data and NOEs and Their Standard Deviation at 500-, 600-, and 750-MHz Spectrometer Frequencies of the Residues in the Amphipathic and Hydrophobic Helices[a]

helix	frequency	R_1 (s^{-1})	dR_1 (s^{-1})	R_2 (s^{-1})	dR_2 (s^{-1})	NOE	SD_{NOE}
A	500	1.70	0.05	8.89	0.34	0.44	0.05
A	600	1.42	0.07	8.53	0.45	0.48	0.08
A	750	1.22	0.08	11.30	0.30	0.62	0.06
H	500	1.43	0.07	15.66	1.34	0.74	0.09
H	600	1.20	0.12	16.20	1.66	0.81	0.15
H	750	0.86	0.15	18.95	1.08	0.82	0.11

[a] For the amphipathic helix (A), the mean value was calculated from the data of residues 9−21, and for the hydrophobic helix (H), residues 27−41 were used.

Anisotropic Rotation. Work by Schurr et al. (1994) indicated that use of the extended model-free approach (eq 8) to interpret the relaxation data may lead to the introduction of internal motions, on the nanosecond time scale, not really present in the considered system. These motions may arise as an artifact when the molecule undergoes anisotropic tumbling so that the extended model-free approach is used outside its domain of validity. To examine this possibility for the present system, we attempted to fit the relaxation data with an anisotropic model.

To be able to include the effect of anisotropic tumbling, the macromolecular structure needs to be included in the analysis (Tjandra et al., 1995). The structure of the micelle−gVIIIp complex is, however, not available other than that we know that the protein consists of two α-helices connected by a hinge region (*vide supra*).

The relaxation parameters of the residues within the individual helices turn out to be very similar. This is not unexpected because the α-helical backbone vectors are almost collinear with the helix axis, making on average an angle of about 15° with it. Therefore, for each of the helices the average of the relaxation parameters was assigned to the total helix (Table 4). In this approach residues 9−21 (13 residues) of the amphipathic helix and residues 27−41 (15 residues) of the hydrophobic helix were taken. This provides a basis for the calculation of the orientation of the helices with respect to the unique axis of the protein−micelle complex. This can be achieved by using the angle between

Table 5: Backbone Dynamical Parameters of the Two Helices of gVIIIp[a]

		amphipathic helix						hydrophobic helix						
τ_c, τ_{eff}	r	model	τ_e (ps)	S^2	S_f^2	θ (deg)	χ^2	model	τ_e (ps)	S^2	S_f^2	θ (deg)	χ^2	χ^2_{tot}
11.5	1.0	III	1200	0.65			61.42	II		1.00			8.46	69.88
11.5	1.0	IV	1500	0.53	0.88		7.90	II		1.00			8.46	16.36
7.5	4.5	V	100	0.80		60	38.98	VI		0.95		30	4.83	43.80

[a] The parameters were determined from models I−VI.

the helix axis and the axial symmetry axis of the system, as well as $r = D_\parallel/D_\perp$, as fitting parameters in a grid search procedure, which is feasible because we obtained a total of nine relaxation parameters per helix segment by using three different spectrometer frequencies. The results are summarized in Table 5.

The grid search procedure was tested with models II, III, and IV, which in fact correspond with the isotropic models 1, 2, and 3 (cf. Table 1) and yield similar answers (Tables 3 and 5). For anisotropic motion (models V and VI, Table 1), an optimal fit is obtained when for the amphipathic helix $\theta = 60°$ and for the hydrophobic helix $\theta = 30°$. In all models used, the best fit was obtained using only S^2 for the hydrophobic helix and using at least two parameters (S^2 and τ_e) for the amphipathic helix. However, in comparison with the isotropic model, the internal correlation time of the amphipathic helix in the anisotropic model reduces to $\tau =$ 100 ps. This is true not only for the real minimum of the selected model (anisotropic ratio $r = 4.5$, Table 5) but also for all other combinations of parameters with an anisotropic ratio between 2.5 and 4.5 (data not shown). In the fits of the same model with smaller anisotropic ratios (1−2) the internal motion correlation time is large (900−1600 ps). Thus, in this approach the original nanosecond internal motion is accommodated in the overall anisotropic motion, as described by Schurr et al. (1994).

However, when comparing the χ^2 values of the simple model-free form and the anisotropic model in Table 5, the more complex model cannot be justified in terms of the *F*-test statistic, which has a value of 2.18 [$F(0.05, 3, 11) = 3.59$]. This is not true when the simple model-free form and the extended model-free form are compared [determined value $= 42.52$, $F(0.05, 1, 13) = 4.67$]. Furthermore, the nanosecond internal motion is already present when the simple model-free approach is applied to the data of the coat protein (Table 5). On the other hand, in the studies of Schurr et al. (1994), the effect of the nanosecond internal motion was only seen when the extended model-free eq 8 was used and was not detected in the simple form of the model-free approach. Finally, we consider the result to be physically irrealistic because $r = D_\parallel/D_\perp = 4.5$, a value which is inconsistent with the possible dimensions of the complex; it cannot be achieved even if the amphipathic helix would be collinear with the hydrophobic helix.

Reduced Spectral Density Mapping. Using eq 6 the spectral density function was calculated at $J(0)$, $J(\omega_N)$, and $\langle J(\omega_H)\rangle$; the parameters derived from the measurements performed at 500 MHz are displayed as a function of residue number in Figure 4. The $J(0)$ and $\langle J(\omega_H)\rangle$ values differ significantly for different parts of the protein, in the same manner as already noticed for the relaxation parameters. This similarity is not very surprising, since $J(0)$ is predominantly determined by R_2 and $\langle J(\omega_H)\rangle$ is determined by the NOE (see eqs 1−3). Recently, Lefèvre et al. (1996) attempted a

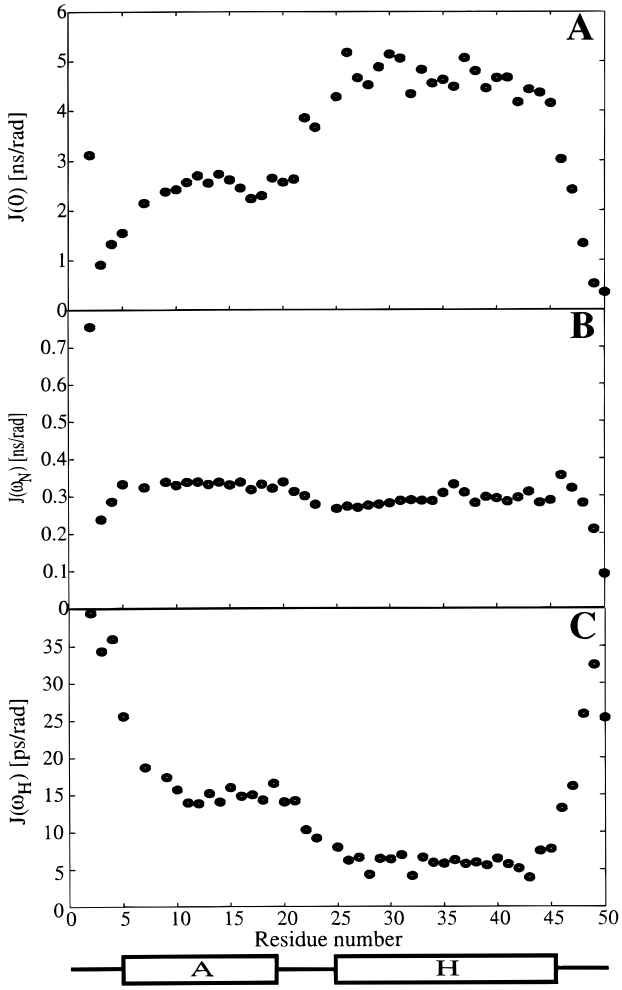

FIGURE 4: Values of the spectral density function versus the residue number of gVIIIp in SDS micelles. The spectral density function was determined at the frequencies (A) 0, (B) ω_N, and (C) $0.87\omega_H$. The secondary structure of gVIIIp is indicated; the box with letter A denotes the amphipathic helix and the box with letter H the hydrophobic helix.

further interpretation of the spectral densities. They constructed plots in which $J(\omega_N)$ or $\langle J(\omega_H)\rangle$ was plotted as a function of $J(0)$ to study the internal mobility of the amide $^{15}N-^1H$ vectors in the GAL4 DNA-binding domain. This turned out to yield a linear relationship between these parameters. The spectral densities obtained for the gene VIII protein (see Figure 4, derived from the 500-MHz measurements), plotted in this manner, are presented in Figure 5 for residues 7−45. The data of the amphipathic helix are represented by crosses, those of the hydrophobic helix are shown by plus signs, and those of the other residues are displayed as circles. It is clear that, except for a few points, the spectral densities of the $^{15}N-^1H$ vectors cluster in two domains, i.e., the vectors in the amphipathic helix fall around $J(0) \approx 2.3$ ns/rad, with $J(\omega_N) \approx 0.33$ ns/rad and $\langle J(\omega_H)\rangle \approx$ 15 ps/rad. The spectral densities of the $^{15}N-^1H$ vectors

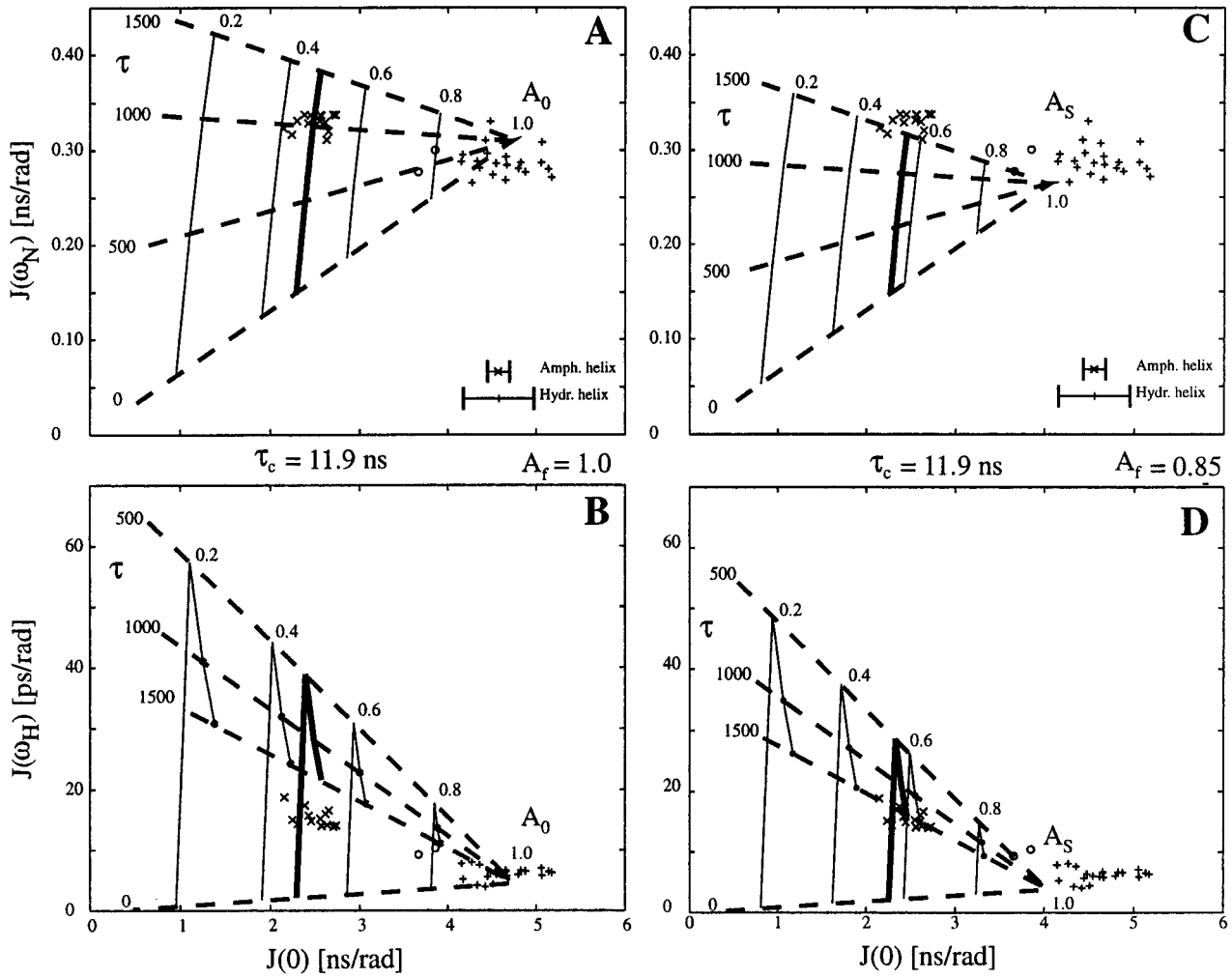

FIGURE 5: Plots of (A, C) $J(\omega_N)$ vs $J(0)$ and (B, D) $\langle J(\omega_H)\rangle$ vs $J(0)$. The experimental data, calculated from eq 6, are represented by crosses for the amphipathic helix (residues 7−21), by plus signs for the hydrophobic helix (residues 25−45), and by circles for the other residues (22 and 23). Theoretical spectral densities represented by the dashed and solid lines were calculated using eq 13 for panels A and B and eq 15 for panels C and D, using τ_c = 11.9 ns and internal correlation times varying between 0 and 1500 ps. The solid lines connect theoretically calculated $J(\omega) - J(0)$ combinations corresponding with the same A_0 or A_s, whereas the dashed lines represent the data for which τ = 0, 500, 1000, and 1500 ps, respectively. A_f = 1 for panels A and B, and A_f = 0.85 for panels C and D. The bold solid line connects the calculated $J(\omega) - J(0)$ combinations for the average value of A_0 derived for the amphipathic helix.

in the hydrophobic helix fall around $J(0) \approx 4.8$ ns/rad, with $J(\omega_N) \approx 0.28$ ns/rad and $\langle J(\omega_H)\rangle \approx 2.5$ ps/rad. From the available data it cannot be concluded that a linear relation, as found by Lefèvre et al. (1996), exists for the coat protein. Nevertheless, it is interesting to elaborate upon this feature. The most simple situation for which one may expect to encounter such a simple relationship is when the spectral density is a linear combination of two Lorentzians:

$$J(\omega) = (^2/_5)\left[\frac{A_0\tau_c}{1+(\omega\tau_c)^2} + \frac{A_1\tau}{1+(\omega\tau)^2}\right] \qquad (12)$$

with $A_1 = 1 - A_0$. We assume that τ_c is the overall correlation time and τ is related to the internal correlation time (e.g., as in the Lipari−Szabo approach, see eq 7). It is easy to show that for this situation

$$J(\omega) = \frac{1-\tau\tau_c\,\omega^2}{N}J(0) + \frac{2\omega^2\tau\tau_c(\tau+\tau_c)}{5N} \qquad (13)$$

with $N = (1+\omega^2\tau_c^2)(1+\omega^2\tau^2)$. Thus, for constant values of τ_c and τ, and for a given value of ω, $J(\omega)$ is a linear function of $J(0)$. The slope of the line is positive for $\tau\tau_c\omega^2 < 1$ and negative for $\tau\tau_c\omega^2 > 1$; for $\tau\tau_c\omega^2 = 1$ the slope is 0, and in a plot of $J(\omega)$ versus ω the Lorentzians cross, i.e., at the particular value of ω where $J(\omega)$ is probed. In Figure 5A,B eq 13 has been plotted for $\omega = \omega_N$ and $\omega = 0.87\omega_H$ for different values of τ with τ_c = 11.9 ns. The solid lines connect calculated points with the same A_0, whereas the dashed lines represent the data for which τ = 0, 500, 1000, and 1500 ps, respectively. It is implicit in this approach that the $^{15}N-^1H$ vectors are subject to the same motional behavior, i.e., their motions can be characterized by the same correlation times. It is obvious that such a situation obtains for the overall motion of the molecule but this is not evident for the internal motion of the individual $^{15}N-^1H$ vectors. This situation may, however, be applicable when the vectors in a certain part of the molecule are subject to the same (diffusional) motion. This is very likely true for the amphipathic helix as suggested by the similarity of the relaxation parameters of its $^{15}N-^1H$ vectors. As mentioned, the dashed straight lines representing eq 13 in Figure 5 arise from linear combinations of two Lorentzians, which means that each point on such a line corresponds with a certain value of A_0. This is illustrated in Figure 5; proceeding from right to left, the values of A_0 decrease from 1 to 0. As

expected for $A_0 = 1$ all lines, corresponding to different values of τ, coincide because at that point the motion characterized by the correlation time, τ, does not contribute. As follows from the foregoing discussion, for constant ω and τ_c the slope of the lines will depend on the values τ (see Figure 5). It is interesting to note that in the $J(\omega_N) - J(0)$ plot $J(\omega_N)$ increases with increasing values of τ, while in the $\langle J(\omega_H)\rangle - J(0)$ plot $\langle J(\omega_H)\rangle$ initially rapidly increases, goes through a maximum for $\tau \approx 500$ ps, and then decreases. This behavior is to be expected, as can be seen in a plot of $J(\omega)$ versus τ (cf. Figure 6). At this point it is interesting to consider the experimental results. As expected the values of the $^{15}N-^{1}H$ vectors in the hydrophobic helix are clustered around the point where the different straight lines cross, i.e., for $A_0 \approx 1$, where the internal motion does not contribute. An interesting situation obtains for the vectors of the amphipathic helix. In the $J(\omega_N) - J(0)$ plot the data points fall around the line representing a correlation time for the internal motion approximately equal to 1000 ps, while from the $\langle J(\omega_H) - J(0)$ plot this correlation time is estimated to be ≈2000 ps. This means that for the vectors in the amphipathic helix the simple model, i.e., $J(\omega)$ is the sum of two Lorentzians, is not applicable and additional internal motions should be allowed for. A simple description of the interpretation of the spectral densities, i.e., linear relationships in the $J(\omega) - J(0)$ plots, may be retained by introducing a scaling factor A_f as indicated in

$$J(\omega) = (^2/_5)\left[\frac{A_f A_s \tau_c}{1 + (\omega\tau_c)^2} + \frac{(A_f(1 - A_s))\tau}{1 + (\omega\tau)^2}\right] \quad (14)$$

There are different possible interpretations for scaling, e.g., the effective $^{15}N-^{1}H$ internuclear distance may differ from the value used above (1.02 Å) (Lipari & Szabo, 1982a; Jarvet et al., 1996) or the presence of very fast internal motion may require the introduction of a scaling factor (Clore et al., 1990a,b). In the latter approach $1-A_f$ is the relative amplitude of the spectral density of the fast internal motion, A_s is that of the "slow" nanosecond internal motion, and $A_f A_s = A_0$ is the amplitude of the spectral density corresponding with the overall motion. Furthermore, τ_c is the correlation time of the overall motion and τ is related to the slow internal motion, τ_s. Thus, $J(\omega)$ is again a linear combination of two Lorentzians. For this situation

$$J(\omega) = \frac{1-\tau_c\tau\omega^2}{N}J(0) + A_f\left(\frac{2\omega^2\tau\tau_c(\tau + \tau_c)}{5N}\right) \quad (15)$$

Thus, for constant values of τ the slope of the straight lines representing the relationship between $J(\omega)$ and $J(0)$ is equivalent to that found for the situation described by eq 12. The factor A_f only scales down $J(\omega)$ by a constant value except for the line characterized by $\tau = 0$. This means that the point where the different lines coincide moves along the $(\tau = 0)$ line to the left by an amount depending on the value of A_f. This is illustrated in Figure 5C,D, in which $J(\omega)$ is plotted versus $J(0)$ for $A_f = 0.85$. It can also be seen in this figure that by choosing $A_f = 0.85$ a situation is generated in which the spectral densities of the the amphipathic helix are clustered close to the $(\tau = 1500)$ line in the $J(\omega_N)$ as well as in the $\langle J(\omega_H)\rangle$ plot.

The interpretation of spectral densities in eqs 13 and 15 mathematically corresponds to mapping of the model-free approach in eqs 7−8 (Lipari & Szabo, 1982a,b; Clore et al., 1990a,b) onto the measured spectral densities. Some physical aspects are immediately transparent in plots as given in Figure 5. We want to mention that in case the motions of the individual $^{15}N-^{1}H$ vectors are characterized by (very) different internal correlation times, $J(\omega)$ is no longer a simple linear function of $J(0)$. Furthermore, the ratio of the slopes of these straight lines for the $J(\omega_H) - J(0)$ and $\langle J(\omega_H)\rangle - J(0)$ plots immediately show whether more than one internal correlation time is needed to derive the $^{15}N-^{1}H$ vector motion. This is seen in Figure 5A,B for the amphipathic helix. A similar difference was observed in the obtained correlation times in the $J(\omega) - J(0)$ plots of the GAL4 DNA-binding domain (Lefèvre et al., 1996). As far as we can tell from the present results, within the theoretical tools currently available for the interpretation of the spectral densities, the model-free approach seems to give an appropriate description even of the motion of a flexible molecule such as the coat protein of filamentous bacteriophage M13.

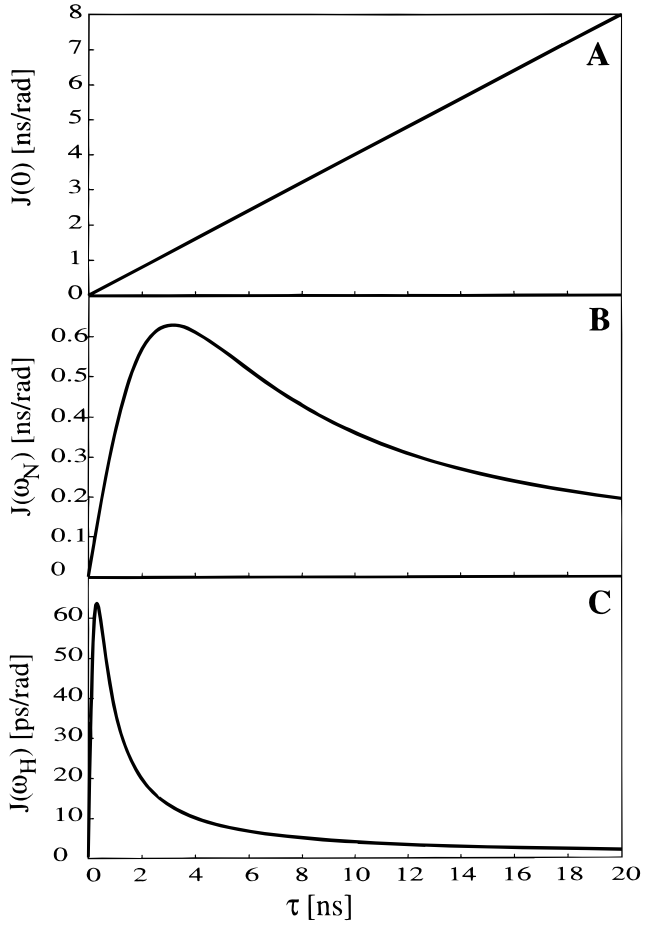

FIGURE 6: Plots of $J(0)$ (A), $J(\omega_N)$ (B), and $\langle J(\omega_H)\rangle$ (C) vs τ. The points were calculated using a single Lorentzian.

Comparison with Other Micellar−Protein Complexes. Recently, Williams et al. (1996) have studied the dynamics of the major coat protein of the related bacteriophage IKe in myristoyllysophosphatidylglycerol (MPG) micelles. This protein consists of 53 residues and shares 19 similar residues at the same positions with the M13 coat protein when the two proteins are aligned at the C-termini. The secondary structure of the coat protein of IKe consist of two α-helical regions as well, corresponding to a amphipathic helix (Asn4−Ser26) and a hydrophobic helix (Trp29−Phe48).

In the study on the IKe coat protein, residues 11−48, which include both the amphipathic and hydrophobic helices, have very similar dynamics. The average order parameter (S^2) for these residues is 0.85. Residue 28 is found to have a lower order parameter than the rest of these residues.

These results are in contrast with our results, which indicate that the amphipathic helix has much more freedom of motion than the hydrophobic helix. This difference may arise from several effects. The length of the amphipathic helix of the IKe coat protein (residues 4−26) is larger than that of the M13 coat protein (residues 6−20). The reduced flexibility of the amphipathic helix of the Ike protein may then result in a stronger interaction between this helix and the MPG micelle than that of the M13 coat protein and the SDS micelle. On the other hand, the different micellar environments may be responsible for the effect or a combination of both effects. The correlation time of the IKe coat protein in MPG micelles is 16 ns, whereas that of the M13 coat protein in SDS micelles is 11.8 ns. Since a MPG molecule has a large head group in comparison with a SDS molecule, a larger micellar size is expected. From the results of the IKe coat protein, it is likely that size of the MPG micelle is such that the amphipathic helix, although exposed to the solvent, is partly immersed into the MPG micelle, having a dynamical behavior similar to the residues of the hydrophobic helix. For the smaller SDS micelles, the amphipathic helix is on the surface of the micelle, thereby obtaining more motional freedom than the hydrophobic helix within the micelle. The relaxation parameters of gVIIIp in DodPCho micelles, whose size is in between those of SDS and MPG micelles, are comparable with those of gVIIIp in SDS micelles, showing more flexibility for the amphipathic helix than for the hydrophobic helix. However, exact information on the motional parameters is not available.

CONCLUSIONS

We have examined the backbone dynamics of the nonglobular major coat protein of bacteriophage M13 using ^{15}N relaxation measurements. We have interpreted the relaxation data using the model-free approach, including the possibility of anisotropic motion, and using reduced spectral density mapping. In the latter method, the spectral densities were interpreted by mapping a linear combination of two Lorentzians onto a $J(0) - J(\omega)$ plot. Given the theoretical tools currently available for the interpretation of the spectral densities, the model-free approach seems to give an appropriate description of the motion of the gene VIII protein. However, it is noted that the dynamics of the amphipathic helix might be more complex than described by the models being applied here, as indicated by the high χ^2 values of some residues in this part of the protein. This may reflect difficulties similar to those encountered by Jarvet et al. (1996), who could not, at the same time, reproduce the spectral density at low and high frequencies.

Our results indicate, as found earlier, that the terminal residues are very mobile. The motion of the hydrophobic helix, located within the micelle, corresponds with the overall tumbling of the protein/micelle complex. The hinge region around residue 22 does not show additional flexibility compared to the two helices. In fact, proceeding from the hydrophobic to the amphipathic helix, a rather abrupt shift in the dynamical parameters occurs. Residue 25 is very restricted in its motion, whereas residue 21 has the same motional flexibility as the other residues in the amphipathic helix. The residues in this helix are subject to extra internal motions with correlation times in the fast nanosecond and picosecond time scales. The extra motions of the ^{15}N−^{1}H vectors in this helix are not due to anisotropic tumbling of the molecule. The motional behavior of the residues within the amphipathic helix is very similar, as beautifully demonstrated by the clustering of the data points in Figure 5. This indicates that the motions of all vectors are correlated, and we interpret this motional freedom as a motion of the amphipathic helix on and away from the surface of the micelle. We surmise that the motion has a functional role and provides the basis for the description of the conformational change of the structure of the protein in the membrane-bound form to that of the coat of the mature phage. Qualitatively similar results have been obtained for the protein in DodPCho micelles.

ACKNOWLEDGMENT

The NMR spectra were recorded at the Dutch SON/NWO National HF-NMR Facility. We thank Mr. J. J. Joordens for technical assistance.

SUPPORTING INFORMATION AVAILABLE

Three tables containing ^{15}N R_1 and R_2 relaxation rates and the heteronuclear NOEs of the measurements performed at (1) 500, (2) 600, and (3) 750 MHz (9 pages). Ordering information is given on any current masthead page.

REFERENCES

Abragam, A. (1961) *The Principles of Nuclear Magnetism*, Clarendon Press, Oxford, England.

Bartels, C., Xia, T., Billeter, M., Güntert, P., & Wüthrich, K. (1995) *J. Biomol. NMR 5*, 1−10.

Bogusky, M. J., Leo, G. C., & Opella, S. J. (1988) *Proteins: Struct., Funct., Genet. 4*, 123−130.

Cavanagh, J., Palmer, A. G., III, Wright, P. E., & Rance, M. (1991) *J. Magn. Reson. 91*, 429−436.

Clore, G. M., Driscoll, P. C., Wingfield, P. T., & Gronenborn, A. M. (1990a) *Biochemistry 29*, 7387−7401.

Clore, G. M., Szabo, A., Bax, A., Kay, L. E., Driscoll, P. C., & Gronenborn, A. M. (1990b) *J. Am. Chem. Soc. 112*, 4989−4991.

Colnago, L. A., Leo, C. G., Valentine, K. G., & Opella, S. J. (1985) in *Biomolecular Stereodynamics, Proceedings of Fourth SUNYA Conversation in the Discipline Biomolecular Stereodynamics* (Sarma, R. H., & Sarma, M., Eds.) Vol. 3, pp 147−158, Adenine Press, Guilderland, NY.

Cross, T. A., & Opella, S. J. (1980) *Biochem. Biophys. Res. Commun. 92*, 478−484.

Dayie, K. T., & Wagner, G. (1994) *J. Magn. Reson., Ser. A 111*, 121−126.

Devore, J. (1982) *Probability and Statistics for Engineering and the Sciences*, Brooks/Cole Publishing Company, Monterey, CA.

Farrow, N. A., Muhandiram, R., Singer, A. U., Pascal, S. M., Kay, C. M., Gish, G., Shoelson, S. E., Pawson, T., Forman-Kay, J. D., & Kay, L. E. (1994) *Biochemistry 33*, 5984−6003.

Farrow, N. A., Zhang, O., Szabo, A., Torchia, D. A., & Kay, L. E. (1995) *J. Biomol. NMR 6*, 153−162.

Henry, G. D., & Sykes, B. D. (1990) *Biochemistry 29*, 6303−6313.

Henry, G. D., & Sykes, B. D. (1992) *Biochemistry 31*, 5284−5297.

Henry, G. D., Weiner, J. H., & Sykes, B. D. (1986) *Biochemistry 25*, 590−598.

Henry, G. D., Weiner, J. H., & Sykes, B. D. (1987a) *Biochemistry 26*, 3619−3626.

Henry, G. D., Weiner, J. H., & Sykes, B. D. (1987b) *Biochemistry 26*, 3626−3634.

Hiyama, Y., Niu, C. H., Silverton, J. V., Bavoso, A., & Torchia, D. A. (1988) *J. Am. Chem. Soc. 110*, 2378−2383.
Ishima, R., & Nagayama, K. (1995a) *Biochemistry 34*, 3162−3171.
Ishima, R., & Nagayama, K. (1995b) *J. Magn. Reson., Ser. B 108*, 73−76.
Jarvet, J., Allard, P., Ehrenberg, A., & Gräslund, A. (1996) *J. Magn. Reson., Ser. B 111*, 23−30.
Kay, L. E., Torchia, D. A., & Bax, A. (1989) *Biochemistry 28*, 8972−8979.
Kay, L. E., Keifer, P., & Saarinen, T. (1992a) *J. Am. Chem. Soc. 114*, 10663−10665.
Kay, L. E., Nicholson, L. K., Delaglio, F., Bax, A., & Torchia, D. A. (1992b) *J. Magn. Reson. 97*, 359−375.
Knippers, R., & Hoffman-Berling, H. (1966) *J. Mol. Biol. 21*, 293−304.
Konings, R. N. H. (1980) *Methods Enzymol. 65*, 795−811.
Konings, R. N. H., Ward, R., Francke, B., & Hofschneider, P. H. (1970) *Nature 226*, 604−607.
Lefèvre, J.-F., Dayie, K. T., Peng, J. W., & Wagner, G. (1996) *Biochemistry 35*, 2674−2686.
Leo, G. C., Colnago, L. A., Valentine, K. G., & Opella, S. J. (1987) *Biochemistry 26*, 854−862.
Lipari, G., & Szabo, A. (1982a) *J. Am. Chem. Soc. 104*, 4546−4559.
Lipari, G., & Szabo, A. (1982b) *J. Am. Chem. Soc. 104*, 4559−4570.
Mandel, A. M., Akke, M., & Palmer, A. G., III (1995) *J. Mol. Biol. 246*, 144−163.
Marvin, D. A., Hale, R. D., Nave, C., & Helmer Citterich, M. (1994) *J. Mol. Biol. 235*, 260−286.
McDonnell, P. A., Shon, K., Kim, Y., & Opella, S. J. (1993) *J. Mol. Biol. 233*, 447−463.
O'Neil, J. D. J., & Sykes, B. D. (1988) *Biochemistry 27*, 2753−2762.
Opella, S., Kim, Y., & McDonnell, P. A. (1994) *Methods Enzymol. 239*, 536−560.
Palmer, A. G., III, Cavanagh, J., Wright, P. E., & Rance, M. (1991a) *J. Magn. Reson. 93*, 151−170.
Palmer, A. G., III, Rance, M., & Wright, P. E. (1991b) *J. Am. Chem. Soc. 113*, 4371−4380.
Palmer, A. G., III, Skelton, N. J., Chazin, W. J., Wright, P. E., & Rance, M. (1992) *Mol. Phys. 75*, 699−711.
Papavoine, C. H. M., Konings, R. N. H., Hilbers, C. W., & Van de Ven, F. J. M. (1994) *Biochemistry 33*, 12990−12997.
Papavoine, C. H. M., Aelen, J. M. A., Konings, R. N. H., Hilbers, C. W., & Van de Ven, F. J. M. (1995) *Eur. J. Biochem. 232*, 490−500.
Peng, J. W., Thanabal, V., & Wagner, G. (1991) *J. Magn. Reson. 95*, 421−427.
Schurr, J. M., Babcock, H. P., & Fujimoto, B. S. (1994) *J. Magn. Reson. Ser. B 105*, 211−224.
Spruyt, R. B., Wolfs, C. J. A. M., & Hemminga, M. A. (1989) *Biochemistry 28*, 9158−9165.
Stonehouse, J., Shaw, G. L., Keeler, J., & Laue, E. D. (1994) *J. Magn. Reson. Ser. A 107*, 178−184.
Tjandra, N., Feller, S. E., Pastor, R. W., & Bax, A. (1995) *J. Am. Chem. Soc. 117*, 12562−12566.
Van de Ven, F. J. M., van Os, J. W. M., Aelen, J. M. A., Wymenga, S. S., Remerowski, M. L., Konings, R. N. H., & Hilbers, C. W. (1993) *Biochemistry 32*, 8322−8328.
Wickner, W. (1988) *Biochemistry 27*, 1081−1086.
Williams, K. A., Farrow, N. A., Deber, C. M., & Kay, L. E. (1996) *Biochemistry 35*, 5145−5157.
Woesner, D. E. (1962a) *J. Chem. Phys. 37*, 647−654.
Woesner, D. E. (1962b) *J. Chem. Phys. 36*, 1−4.

BI962650E